Rock Mechanics and Rock Engineering
https://doi.org/10.1007/s00603-023-03670-z

ORIGINAL PAPER

The Effect of Weathering on the Mineral Grains and Macroscale Young's Modulus of Granites

Jiangmei Qiao[1] · Mengmeng Nie[1] · Qi Zhao[2] · Quansheng Liu[1] · Xuhai Tang[1,3]

Received: 16 August 2023 / Accepted: 7 November 2023
© The Author(s), under exclusive licence to Springer-Verlag GmbH Austria, part of Springer Nature 2023

Abstract

Weathering process leads to changes in mineral composition, microdefects and mechanical properties of mineral grains, which has a significant impact on the macroscale mechanical properties of granitic rocks. In this paper, four granitic samples with different weathering degrees were investigated using microscale rock mechanics experiments (micro-RME), macroscale rock mechanics experiments (macro-RME) and accurate grain-based model (AGBM). The following conclusions can be achieved. First, quartz is erosionally resistant compared to feldspar and biotite. The weathering products of feldspar and biotite are sericite and chlorite, respectively. Second, with the increasing of weathering degree, the volume fractions of quartz and weathering products increase, meanwhile the volume fractions of feldspar and biotite decrease. Third, during the weathering process, Young's modulus of quartz and feldspar almost keep constant, however, Young's modulus of biotite decreases significantly. Fourth, the weathering process significantly increases the volume of microdefects, including pores and microcracks. Finally, from the viewpoint of the weathering effect, we discovered a negative correlation between quartz content and the macroscale Young's modulus of granites.

Highlights

- The effect of weathering on the granite at multiscale has been investigated.
- The quartz is erosionally resistant compared to feldspar and biotite.
- During weathering process, the strength of quartz and feldspar almost keep constant, however the strength of biotite decreases significantly.
- During weathering process, the volume fractions of quartz and weathering products increase, and the feldspar and biotite decrease.
- The weathering process significantly increases the volume of microdefects, including pores and microcracks.

Keywords Weathering · Granites · Weathering product · Minerals · Multiscale

1 Introduction

Granites widely distributed on Earth and are extensively used for engineering construction. Weathering process has a significant impact on the mineral composition, porosity and microcracks of rocks, which leads to the deterioration of their macroscale mechanical properties. There are numerous engineering disasters associated with weathering effects, such as the landslide induced by rainfall

✉ Xuhai Tang
xuhaitang@whu.edu.cn

[1] School of Civil Engineering, Wuhan University, Wuhan 430072, China

[2] Department of Civil and Environmental Engineering, The Hong Kong Polytechnic University, Hong Kong 100872, China

[3] Wuhan University Shenzhen Research Institute, Shenzhen 518108, China

Published online: 11 December 2023

(Xu et al. 2020) and the rockfall induced by freeze–thaw weathering in cold regions (Tang et al. 2022a; Kanno et al. 2023). Understanding the impact of weathering on the mechanical properties of granites at multiscale is crucial for predicting their long-term performance and durability.

Over the past few decades, extensive research has discussed the influence of weathering on the macroscale mechanical properties of rocks. Moye (1955) divided the weathering effect into six grades, which may be the most widely used classification system. The weathering grade I represents fresh rock and weathering grade VI represents soil. Heidari et al. (2013) proposed a weathering classification system for granitic rocks in Malaysia with tropical climatic condition, using physic-mechanical parameters, including strength retention index, P-wave velocity, porosity, point load strength index and Brazilian tensile strength. After investigating forty sections in Malaysia, Abad et al. (2016) identified the weathering zones with various granitic rocks based on joint characteristics, corestone occurrence, rock/soil ratio, mass homogeneity and the color of rocks. Wang et al. (2016) investigated the dynamic mechanical properties and deterioration of red sandstone subjected to repeated thermal shock weathering. By laboratory disintegration tests on natural granite residual soil collected from different depths (3.5–17.5 m), Liu et al. (2022) established a framework for investigating the disintegration behavior of residual soils affected by weathering and provided a comprehensive dataset of natural granite residual soil. By conducting durability test cycles on three different types of granites using quasistatic compressive test and acoustic emission monitoring, Zhou et al. (2023) revealed the damage characteristics of rocks subjected to freeze–thaw weathering, which is potentially useful to predict rock failure in cold region.

Both physical weathering and chemical weathering lead to changes in minerals and the formation of microdefects, including pores and microcracks. Basu et al. (2009) pointed out that the deterioration of macroscale mechanical properties during weathering is attributed to the alteration of minerals, the disruption of rock skeleton and increased microdefects. By examining the petrography and geochemistry of Utla granites, Sajid et al. (2014) found that the extensive recrystallization and associated mineralogical changes are the reasons for the strength reduction. Huang et al. (2021) pointed out that, the weakening of grain contact stiffness leads to the weakening of macroscale mechanical characteristics. Xu et al. (2020) investigated the influence of water immersion on the mechanical properties of minerals in a shale weak interlayer, which pointed out that the softening of shale is mainly due to the collapse of clay minerals, such as chlorite. This result was then used to predict the landslides in slopes with shale weak interlayers.

Some numerical models have been developed to establish an accurate relationship between mineral grains and macroscale mechanical properties. During the last decade, many researchers have investigated the mechanical properties of rocks at grain scale. Lan et al. (2010) developed a grain-based distinct element model to discuss the effect of heterogeneity on microscale tensile behavior of brittle rock under compression loading. Based on Grain-Based Model (GBM) and microscale experiment, Mahabadi et al. (2012, 2014) illustrated that heterogeneity and microcracks significantly affected the tensile strength and failure behavior of rocks. In the context of traditional GBM (Peng et al. 2017, 2018), the distribution, geometry and mechanical properties of rock-forming minerals are inaccurate. Without microstructure testing (e.g., TIMA), the geometry of rock-forming minerals in traditional GBM is usually simplified using Voronoi meshes based on the statistical grain size distribution. Without micromechanical testing (e.g., nanoindentation), the method of numerical calibration is typically used to roughly estimate the mechanical properties of minerals. Recently, the accurate grain-based model (AGBM) was developed to address the above-mentioned disadvantages of traditional GBM (Tang et al. 2022b). AGBM has also been successfully used to estimate the mechanical properties of fragmental granites (Tang et al. 2022b; Xu et al. 2023) and HaH 346 meteorites (Tang et al. 2023).

This study aims to investigate the influence of weathering on the mineral composition, microstructure, micro- and macro-scale mechanical properties of granites. Four granite samples with different weathering degrees were analyzed. Their mineral composition and microstructure were characterized using an optical microscope and TESCAN Integrated Mineral Analyzer (TIMA). The Young's modulus of rock-forming minerals was measured using nanoindentation testing. Subsequently, accurate grain-based models (AGBMs) and macroscale experiments were used to achieve macroscale Young's modulus of these samples. Finally, the relationship between macroscale Young's modulus and some indexes was established.

2 Materials and Methodologies

2.1 Four Granitic Samples with Different Weathering Degrees

Four granitic samples with different weathering degrees were collected, as shown in Fig. 1. The first granite specimen is fresh Bukit Timah granite, which was collected from the Mandai area in the central part of Singapore. This granite is a light gray coarse-grained granodiorite without visible pores

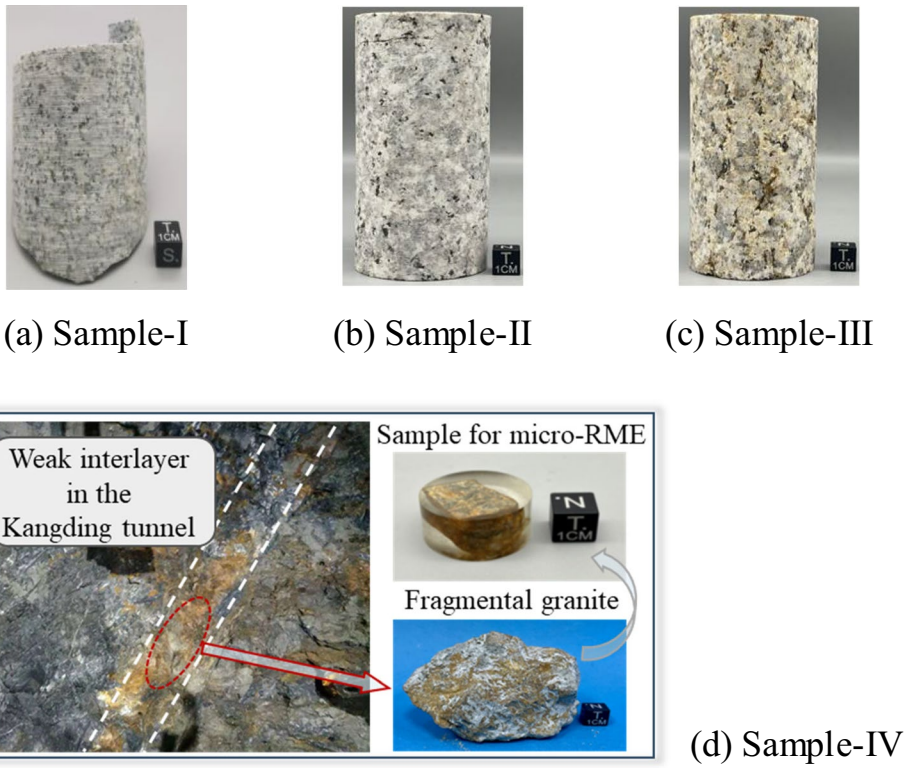


Fig. 1 Four granitic samples with different weathering degrees

and microcracks. According to the weathering classification (Martin and Henchert 1986), this specimen is classified as grade I and named as Sample-I. The second granite specimen was drilled from Jining, China. It is slightly weathered, with slight discoloration and a few visible cracks (Fig. 1b), which is classified as grade II and named as Sample-II. As shown in Fig. 1c, the surface of the third granite specimen exhibits complete discoloration, with significantly developed microcracks, which is classified as grade III and named as Sample-III. Sample-II and Sample-III were collected from the same area with different depths. The fourth specimen was collected from the weak interlayer in the Kangding No.2 tunnel. As shown in Fig. 1d, this sample is yellowish-brown and fragmental, but it does not slake when immersed in water. According to the weathering classification (Martin and Henchert 1986), this sample is classified as grade IV and named as Sample-IV.

2.2 Microscale Rock Mechanics Experiment (Micro-RME)

As shown in Fig. 2, the microscale Rock Mechanics Experiment (micro-RME) system was developed to test the microstructure and microscale mechanical properties of rocks. This system includes optical microscopy, TESCAN Integrated Mineral Analyzer (TIMA) and nanoindentation testing. Both optical microscopy and TIMA were used to obtain the microstructure (e.g., microcracks) and mineral distributions of rocks. The nanoindentation testing was used to obtain the mechanical properties of rock-forming minerals.

It is noticed that optical microscopy and TIMA have their own advantages. The testing of optical microscopy is cheaper and more convenient, so it is able to test massive rock samples to reduce the influence of anisotropy. However, sometimes it is difficult to distinguish the boundaries of mineral grains based on the color information achieved by optical microscopy. The testing of TIMA is able to distinguish the boundaries of mineral grains accurately, however, it is relatively expensive.

(1) Materials preparation for Micro-RME.

Four cubic samples were prepared for micro-RME, with a size of 20 mm × 20 mm × 5 mm. However, Sample-IV is fragmental and narrow, making it difficult to be further cut and polished. Therefore, the entire Sample-IV was cast in resin to enhance its structural fixation, as shown in Fig. 1d. Subsequently, the surface of each specimen was polished using a polisher (Ecomet 250 Buehler) with silicon carbide (SiC) papers of different grain fineness, including P800, P1200, P2500, and P5000. Additionally, to minimize surface roughness, an extra fine alumina suspension was used for further polishing before nanoindentation testing. Finally, the surfaces of all specimens were cleaned ultrasonically.

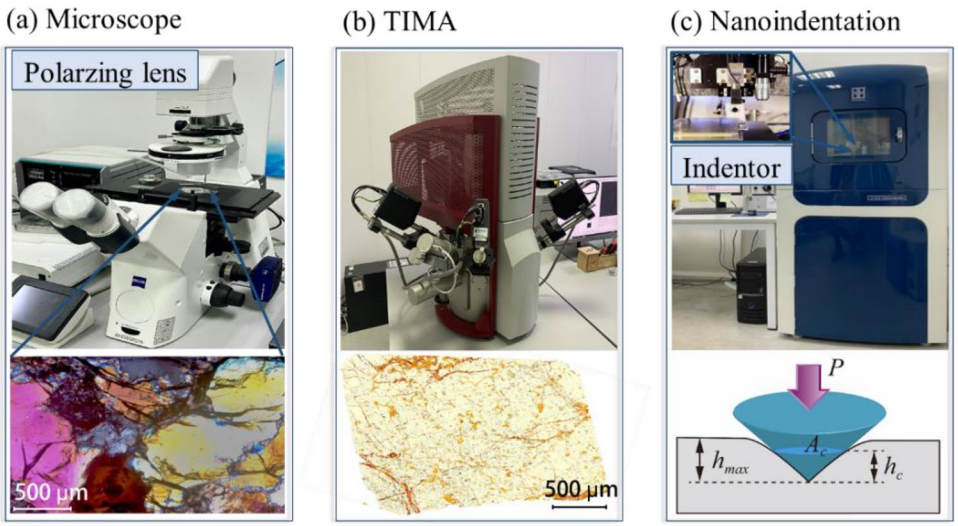


Fig. 2 Microscale Rock Mechanics Experiment (micro-RME) system. **a** Optical microscope; **b** TESAN Integrated Mineral Analyzer (TIMA FEG3 LMH); **c** Hysitron TI950 TriboIndenter System

(2) Measuring the microstructure using an optical microscope.

Polarization optical microscopy is used to examine the microstructure, including microcracks, pores, bedding and minerals. By orthogonal polarization light, it is able to obtain the morphology and distribution of minerals, cleavage, bedding, and microdefects (Fig. 2a). In this work, thin sections were prepared for orthogonal polarization optical microscopy testing.

(3) Measuring the microstructure using TIMA.

TESCAN Integrated Mineral Analyzer (TIMA) is an automated mineral quantitative analysis system used to accurately determine the mineral composition, particle size, and distribution of examined materials. As shown in Fig. 2b, this technique combines calibrated back-scattered electron (BSE) images and energy-dispersive X-ray spectroscopy (EDX) to efficiently identify the mineral components (Santoro et al. 2014; Hrstka et al. 2018).

(4) Measuring Young's modulus of minerals using nanoindentation testing.

Nanoindentation is a well-established technique to obtain the mechanical properties of materials. Since the mid-1970s, nanoindentation has been widely used to test the microscale mechanical properties of materials (Oliver and Pharr 1992; Oyen 2013). Recently, this technology has been successfully applied to investigate the mechanical properties of minerals in rocks (Luo et al. 2020; Li et al. 2021; Tang et al. 2022b).

Berkovich diamond probe tip is used to contact the surface of samples (Fig. 2c). Figure 3 displays a typical load-depth curve captured throughout the indentation process. The Young's modulus E of the sample is calculated as (Oliver and Pharr 1992):

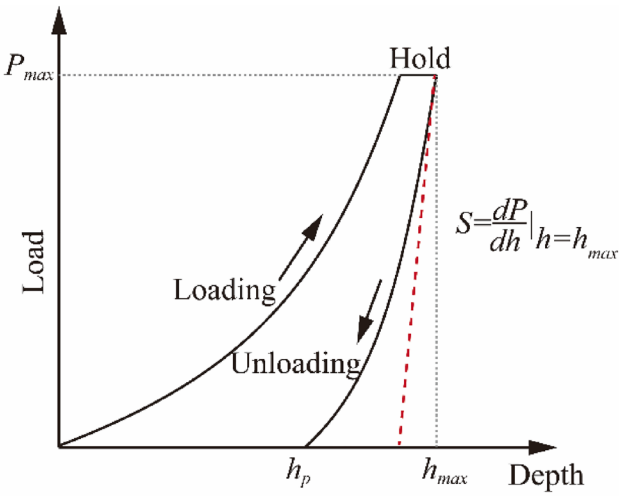


Fig. 3 Typical load-depth curve in nanoindentation testing

$$E = \left(1 - \nu^2\right)\left[\frac{1}{E_r} - \frac{1 - \nu_i^2}{E_i}\right]^{-1} \tag{1}$$

where ν is the Poisson's ratio of the sample. E_i and ν_i are Young's modulus and Poisson's ratio of the Berkovich indenter. E_r is the reduced modulus, which is calculated as:

$$E_r = \frac{\sqrt{\pi}}{2\beta\sqrt{A_c}}S \tag{2}$$

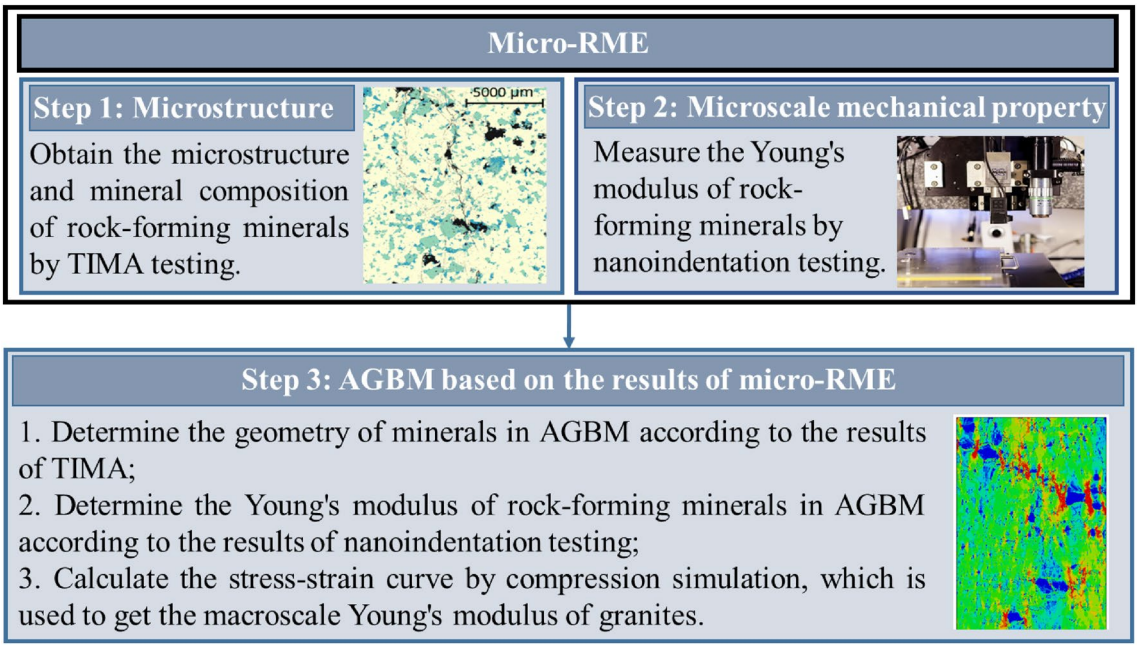


Fig. 4 Determine the macroscale Young's modulus using AGBM and micro-RME

where β is set to 1.05 as the correction factor. A_c is the contact area. S is the stiffness of the unloading curve slope (see Fig. 3) and can be calculated as:

$$S = \left.\frac{dP}{dh}\right|_{h=h_{\max}} \tag{3}$$

where P is the loading force; h is the indentation depth, and $h_{\max}$ is the maximum indentation depth.

In this work, Young's modulus of rock-forming minerals was obtained through nanoindentation testing using the Hysitron TI950 Tribolndenter system. Firstly, the load force was increased linearly to a maximum load of 4 mN at a constant loading rate of 0.8 mN/s. Secondly, the load was held constant for 2 s. Thirdly, the load force decreased linearly at a rate of 0.8 mN/s. To avoid the influence of heterogeneity and anisotropy, four indent matrices were conducted for each mineral. Each indent matrix consists of 5×5 indentation points, with a spacing of 10 μm. The experimental frequency plots of Young's modulus were fitted using the probability density function (PDF). According to existing Ref. (Randall et al. 2009), when the particle size exceeds 1 μm, there is no obvious effect of particle size on the results of nanoindentation testing. To avoid the effect of grain size, we chose relatively large mineral grains for nanoindentation testing.

2.3 Accurate Grain-Based Model (AGBM)

The accurate grain-based model (AGBM) was developed to obtain Young's modulus of small and any-shaped rock samples based on the results of micro-RME. The flowchart to generate AGBMs is shown in Fig. 4. First, based on the accurate mineral distribution images obtain by TIMA, the types of computational element were achieved. Second, based on the results of nanoindentation testing, Young's modulus of computational element was achieved for AGBM. Third, based on the established AGBM, a series of uniaxial compression simulations were performed to generate a stress–strain curve. This computational model was assumed to be a plane strain. The macroscale Young's modulus of this rock sample can be solved according to the slope of stress–-strain curve. The advantages of AGBM include: (1) The results of TIMA ensure that the AGBM is able to precisely capture mineral volume fraction, mineral morphology, the occlusal morphology between minerals, mineral size, and the ratio of maximum to minimum mineral size; (2) The results of nanoindentation testing ensure that the AGBM is able to precisely capture the mechanical properties of rock-forming minerals.

2.4 Macroscale Rock Mechanics Experiment (macro-RME)

Macroscale Rock mechanics Experiment (macro-RME), such as uniaxial/triaxial compression tests and Brazilian tests, are well-developed and widely used to obtain the mechanical parameters of rocks (Chen et al. 2017; Yang et al. 2019). In this work, the macroscale mechanical properties of Sample II and III were obtained using uniaxial and triaxial compression tests. According to the standard recommended

Table 1 The volume fraction of rock-forming minerals in four samples

Mineral	Sample-I	Sample-II	Sample-III	Sample-IV
Quartz	30.40%	74.09%	78.00%	80.00%
Feldspar	57.74%	20.20%	14.75%	0
Biotite	11.42%	5.03%	4.86%	0
Weathering products (Chlorite/Sericite/Calcite)	0.09%	0.18%	0.89%	15.00%
Microdefects	0.35%	0.50%	1.50%	5.00%

by ISRM (Fairhurst and Hudson 1999), the samples were processed into cylinders 100 mm in height and 50 mm in diameter. Triaxial tests were conducted with the confining pressures of 5, 10, 20, and 30 MPa (two at each). A constant loading rate of 0.06 mm/min was used until the specimen failed. 3 uniaxial and 8 triaxial compression test samples were used for Sample II and Sample III, respectively. Additionally, the macroscale Young's modulus of Sample-I was obtained from existing references (Tang et al. 2022b; Wong and Maruvanchery 2016), which is 41.78 GPa. Because Sample-IV was taken from the weak interlayer, it was challenging to process it into a standard sample for traditional macro-RME. Therefore, the macroscale Young's modulus of Sample-IV is obtained by AGBM with the results of micro-RME.

3 The Influence of Weathering on Mineral Grains

3.1 The Influence of Weathering on the Mineral Composition

In this section, the mineral composition of the four samples was quantitatively analyzed using TIMA. The testing was conducted at Chengpu Geological Testing Co. Ltd, Langfang, China. Based on the TIMA results, the volume fractions of different minerals in the four samples are presented in Table 1. The fresh granites in this work mainly consist of three rock-forming minerals: quartz, feldspar and biotite. With the increasing weathering degree, weathering products appear in samples, such as calcite, sericite, chlorite and other opaque clay minerals.

As shown in Fig. 5, there is a noticeable increase in the proportion of quartz during the weathering process. This is attributed to the fact that quartz is highly resistant to weathering. This observation is consistent with previous studies on granite residual soil (Liu et al. 2022), where quartz was found to be the predominant mineral composition.

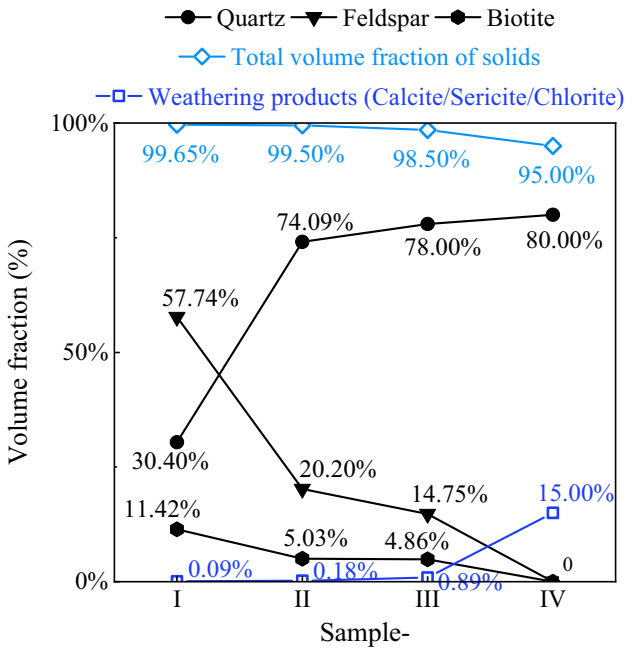


Fig. 5 The mineral volume fraction varies with different weathering degrees

Conversely, feldspar undergoes alteration and decomposition into weathering products, such as sericite, leading to a decrease in its volume fraction. In Sample III, the sericite is the predominant weathering product. In Sample IV, the weathering products include sericite and calcite.

3.2 The Influence of Weathering on Microstructure

The microdefects, including pores and microcracks, were characterized using the optical microscope and TIMA. As shown in Fig. 6a, there is no obvious microdefect in Sample-I, and there is also no obvious weathering product between different rock-forming mineral grains (Fig. 7a). As the increasing weathering degree, the volume of pores and microcracks proportionally increases. The mineral grains become fragmented, meanwhile the microcracks develop, particularly in areas where weathering products accumulate. In Sample IV, these microcracks and weathering products form a discontinuous network throughout the entire rocks, as shown in Fig. 6d.

In Fig. 7, microscopic photographs of four granites at 50 × and 200 × magnifications are presented. In Sample-I (Fig. 7a), the grains exhibit a closely interlocking structure. The boundaries between different grains are clear and distinct. In Sample II (Fig. 7b), the mineral grains remain relatively intact, with little weathering products filling between different grains. As shown in Sample-III (Fig. 7c), intragranular microcracks appear and the mineral grains become fragmented, meanwhile a significant amount of weathering

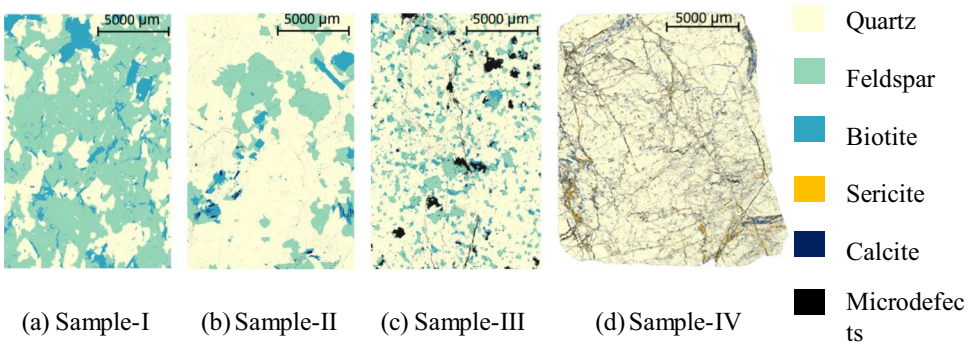


Fig. 6 Mineral composition and microstructure of four granite samples

products and microdefects fill the gaps between different mineral grains. In Sample-IV (Fig. 7d), microcracks develop extensively, ranging in width from 10 μm to 40 μm, and form a discontinuous network. These microcracks are filled with opaque debris, including sericite and clay minerals, possibly derived from plagioclase transformation. The increasing of weathering products makes the color of thin sections present yellowing.

3.3 The Influence of Weathering on the Young's modulus of Rock-Forming Minerals

3.3.1 Quartz

The typical load-depth curves of quartz are shown in Fig. 8. During the indention process, the penetration depth exceeds 100 nm and reaches a maximum of 150 nm. Due to the hardness of the quartz grains, the residual indentations on the quartz surface are shallow. The Young's modulus of quartz in the four samples are 96.81, 103.52, 95.86 and 102.58 GPa, respectively (see Fig. 9). The weathering does not have an effect on Young's modulus of quartz. These findings indicate that quartz is erosionally resistant and does not significantly contribute to the reduction of granitic macroscopic mechanical properties. In the previous Ref. (Mahabadi et al. 2014), the elastic modulus of quartz measured using nanoindentation testing was 99.30 ± 3.65 GPa, which is similar to our results.

3.3.2 Feldspar

In Fig. 10, the typical load-depth curves of feldspar are displayed. The maximum penetration depth of feldspar exceeds 200 nm, indicating lower hardness compared to quartz. The experimental histograms of nanoindentation on feldspar in Sample-I, II and III are shown in Fig. 11. The presence of various mineral phases of feldspar, including plagioclase, orthoclase, and albite, results in discrete load-depth curves and a multi-peak distribution in the experimental histograms. The calculated Young's modulus of feldspar in Sample-I, II and III are 69.50, 68.32 and 67.54 GPa, respectively, which are shown in Table 2. Because Sample-IV is completely weathered, there is no feldspar and biotite. There is no significant correlation between Young's modulus of feldspar and the degree of weathering. In previous Ref. (Mahabadi et al. 2014), the elastic modulus of feldspar measured using nanoindentation testing was 56.37 GPa.

3.3.3 Biotite

The typical load-depth curves of biotite are shown in Fig. 12. The load-depth curves of biotite presented a stepped shape and were not smooth, therefore the measured Young's modulus data of biotite is very discrete (Zhang et al. 2013). Meanwhile, the penetration depth of biotite all exceeds 250 nm and the maximum exceeds 350 nm, which shows a lower stiffness compared to feldspar. The Young's modulus of biotite in Sample-I, II and III are 49.85, 30.46, and 17.32 GPa, respectively, as shown in Fig. 13. With the weathering degrees increase, the Young's modulus of biotite decreases significantly. In previous Ref. (Mahabadi et al. 2014), the elastic modulus of biotite measured using nanoindentation testing was 17.21 GPa.

3.3.4 Weathering Products

The Young's modulus of weathering products, including calcite, sericite, and chlorite was measured by nanoindentation testing (Fig. 14). In Sample-II, the main weathering product is calcite, followed by a small amount of sericite, chlorite and clay minerals. Young's modulus of calcite in Sample II is 38.32 GPa. In Sample III, the main weathering product is sericite, followed by a small amount of calcite. Young's modulus of sericite in Sample-III is 20.34 GPa. In Sample IV, the main weathering products is calcite and sericite. Young's modulus of calcite and sericite in Sample-IV are 35.35 GPa and 14.94 GPa, respectively. It can be observed that Young's modulus of the same weathering products does not undergo significant change during the weathering process. However, the total volume fractions of these weathering products increase.

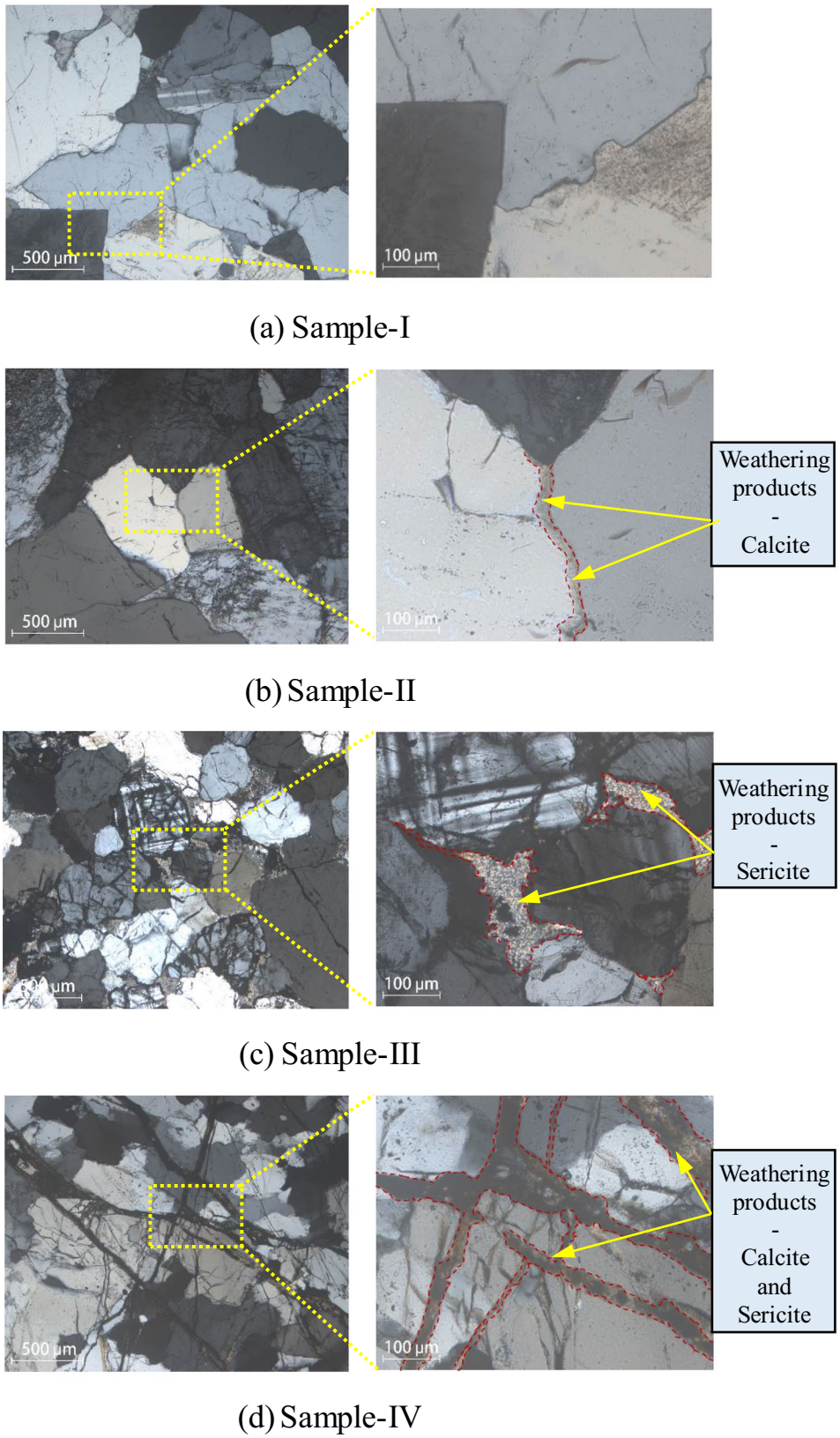


Fig. 7 Photomicrographs of four granitic samples

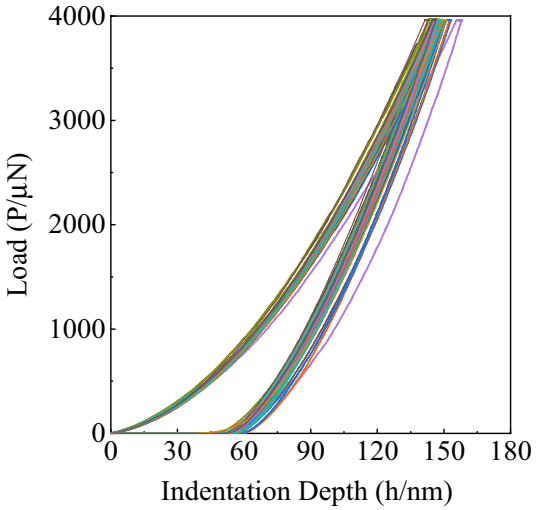


Fig. 8 Typical load-depth curves of quartz

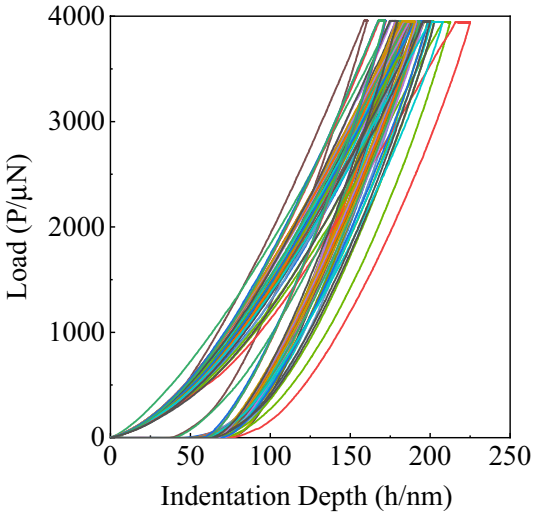
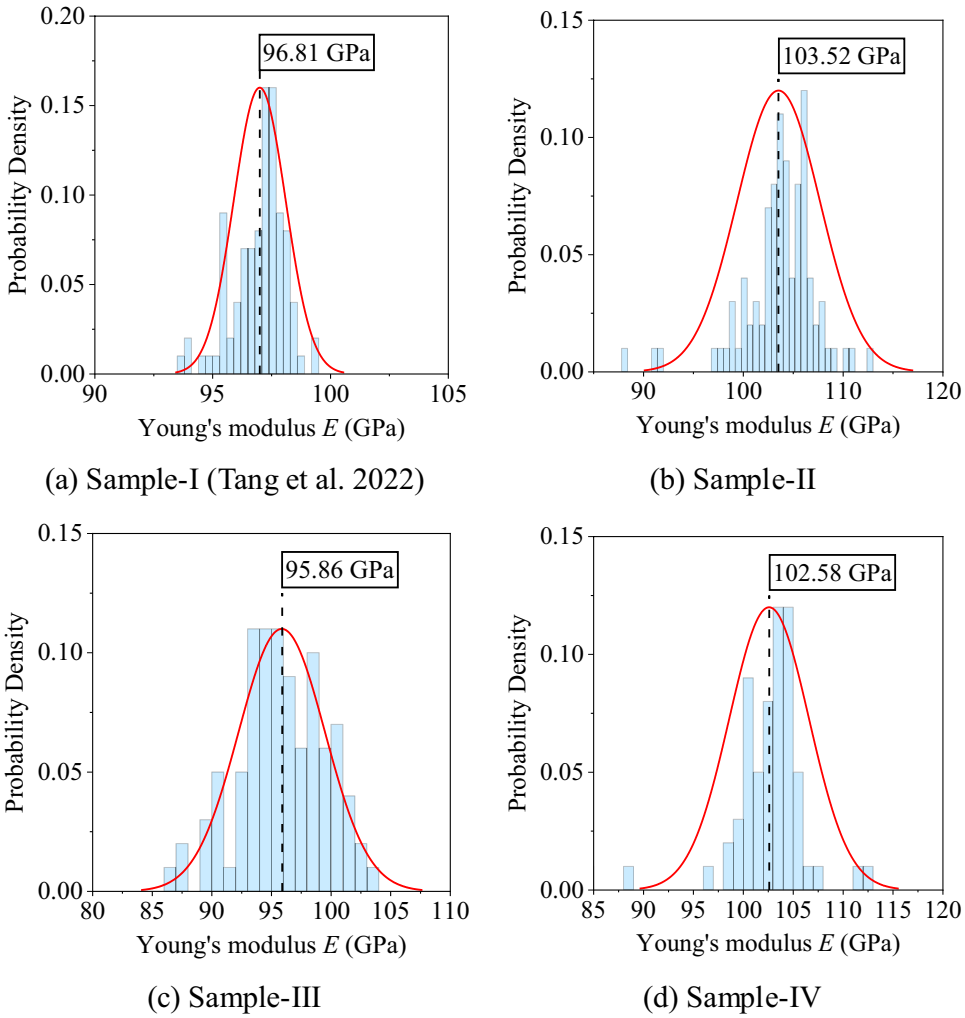


Fig. 10 Typical load-depth curves of feldspar

Fig. 9 Young's modulus results of quartz using nanoindentation testing



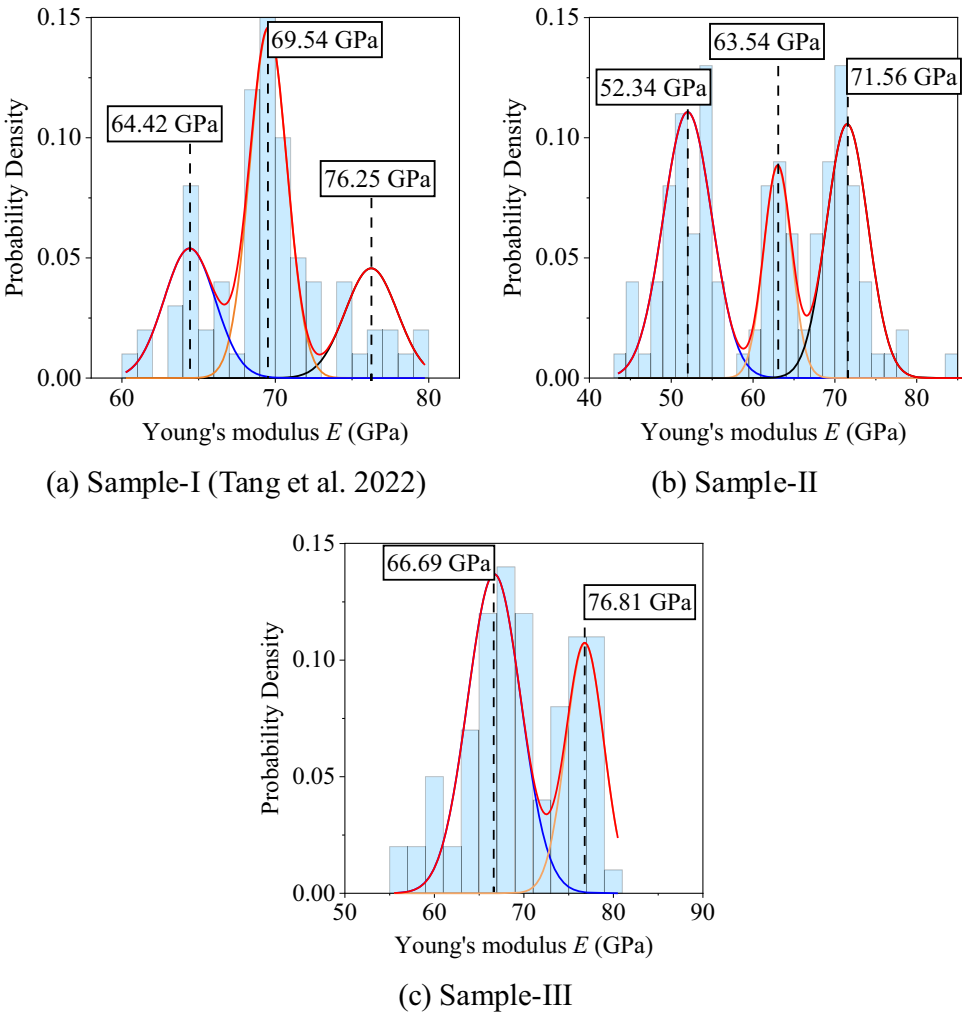
4 The Influence of Weathering on Macroscale Mechanical Properties of Granites

4.1 Measuring Young's Modulus of Sample-I, II and III Using Macro-RME

In this work, the uniaxial and triaxial compression tests were used to obtain the macroscale mechanical properties of Sample II and III. Meanwhile, the macroscale mechanical properties of Sample-I were obtained from existing Ref. (Tang et al. 2022b; Wong and Maruvanchery 2016). The macroscale mechanical properties, including density, Poisson's ratio and Young's modulus of these three samples were summarized in Table 3. With the increasing of weathering degrees, both the density and Young's modulus decrease. Macroscale Young's modulus shows a notable decrease of 65.1% from Sample I to III, while Poisson's ratio experiences a significant increase from Sample II to III. These results show that weathering process has a significant impact on the macroscale mechanical properties of granites.

4.2 Calculating Young's modulus of Sample-IV Using Micro-RME and AGBM

As described in our previous work in Tang et al. (2022b), the accurate grain-based model (AGBM) based on the results of micro-RME is able to achieve Young's modulus of granites properly. Because Sample-IV is completely weathered, it was challenging to process it into a cylindrical standard sample for traditional macro-RME. Therefore, Young's modulus of Sample-IV was estimated using AGBM based on the results of the previous micro-RME. The precise mineral geometry and microstructure distribution used for AGBM modeling are derived from TIMA results in Sect. 3.2. The Young's modulus of computational elements in AGBM was set according to the results of nanoindentation testing (see Table 2) and TIMA. The computational domain of AGBM was extracted from Fig. 6d, and the dimensions were 20 mm



(a) Sample-I (Tang et al. 2022)

(b) Sample-II

(c) Sample-III

Fig. 11 Young's modulus results of feldspar using nanoindentation testing

Table 2 Young's modulus (GPa) of rock-forming minerals obtained by nanoindentation testing on four samples

Mineral	Sample-I	Sample-II	Sample-III	Sample-IV
Quartz	96.81	103.52	95.86	102.58
Feldspar	69.50	68.32	67.54	/
Biotite	49.85	30.46	17.32	/
Calcite	/	38.32	/	35.35
Sericite	/	/	20.34	14.94

in length and 10 mm in width. The established AGBM of Sample-IV is shown in Fig. 15.

Using the established AGBM, a series simulations of compression testing were conducted to obtain the stress–strain curve. The computational model was assumed to be in plane strain. Same to the parameters in Ref. (Tang et al. 2022b), a vertical displacement of 0.2 m was imposed on the upper boundary of the established models. Additionally, fixed vertical constraints were applied to the bottom boundary, while fixed horizontal constraints were added to the left and right sides.

The simulated stress distributions in Sample IV are presented in Fig. 16. The stress concentration phenomenon primarily occurs in regions where weak materials accumulate, such as calcite and sericite, which will lead to crack development. The calculated Young's modulus of sample-IV is 10.52 GPa (see Table 3).

5 Estimate the Young's Modulus of Weathered Granites According to the Content of Quartz

In this section, the relationship between the mineral content and macroscale Young's modulus is investigated, which is potentially useful in some situations. In 2021, the US National Aeronautics and Space Administration (NASA)'s Perseverance rover failed to drill and capture Martian rocks, because the knowledge about the mechanical properties of Martian rocks is limited (Witze 2021a, b). Therefore, some researchers tried to estimate the excavatability of Martian rocks using minerology information, including SiO_2, which can be achieved by spectral signal (Peters et al. 2018; Jacob et al. 2020). However, as mentioned in the recent reference (Peters et al. 2018), "Conclusive evidence linking minerology to the rock strength at Gale crater on Mars remains elusive". It is noticed that the previous conclusive evidence linking the quartz content to rock strength remains elusive, primarily due to the inherent heterogeneity and anisotropy of granites. Several researchers have discovered a positive correlation between the quartz content and the strength of granites (Hassan et al. 2019; Askaripour et al. 2022). On the contrary, several researchers have discovered a negative correlation between quartz content and the strength of granites (Sousa 2013; Du et al. 2022).

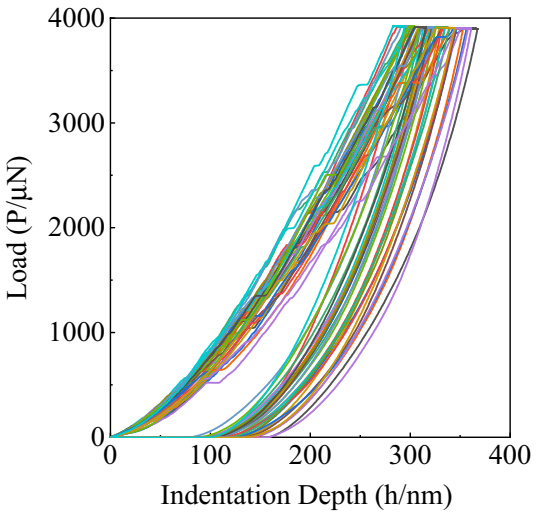


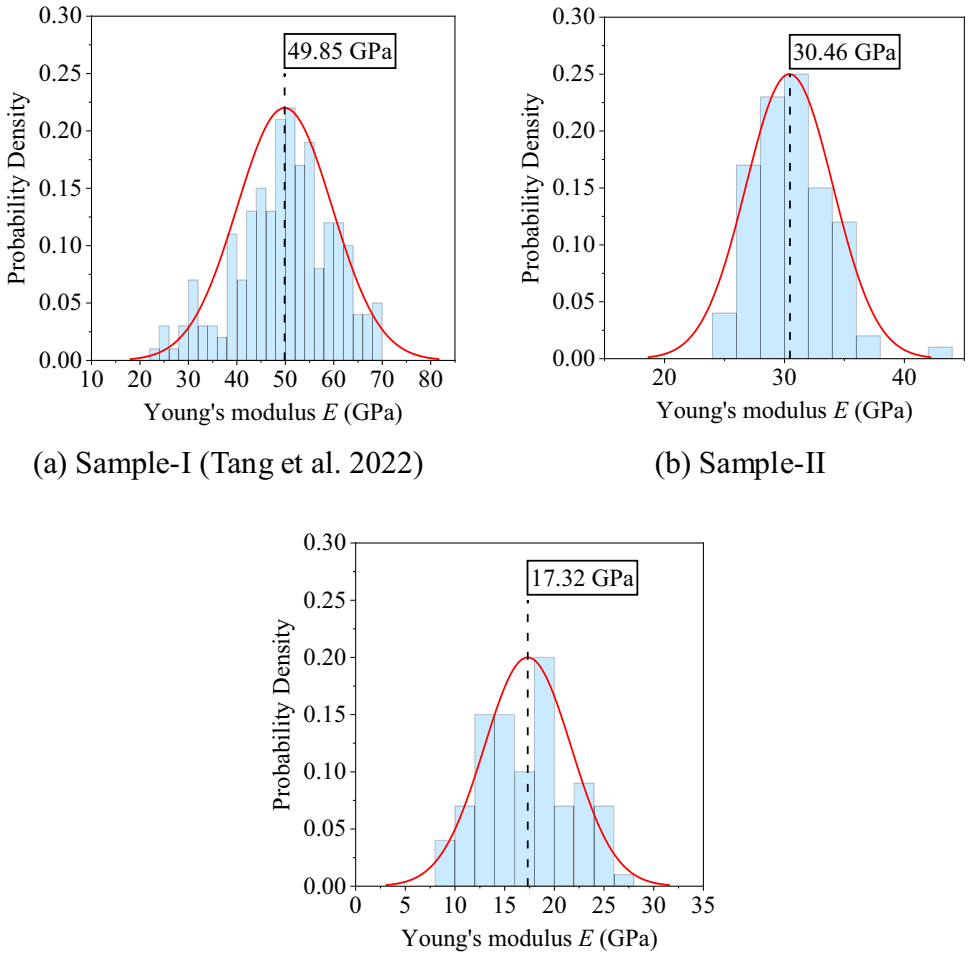
Fig. 12 Typical load-depth curves of biotite

As shown in Table 4, the Pearson correlation coefficient is used to quantitatively analyze the relationship between different indexes. The Pearson correlation coefficient can be calculated as:

$$r = \frac{\sum_{i=1}^{n}(x_i-\bar{x})(y_i-\bar{y})}{\sqrt{\sum_{i=1}^{n}(x_i-\bar{x})^2\sum_{i=1}^{n}(y_i-\bar{y})^2}} \tag{4}$$

where x_i and y_i are the individual data points of the two variables. $\bar{x}$ and $\bar{y}$ are the means of the two variables. In this work, the total number of studied samples $n=4$. The Pearson correlation coefficients are between -1 and 1. When $r=1$, it indicates a perfect positive linear correlation. When $r=-1$, it indicates a perfect negative linear correlation. When $r=0$, it indicates there is no consistent linear relationship between them.

As shown in Table 4, all the absolute values of r are greater than 0.5, indicating a strong correlation among the studied indexes. There is a positive correlation between the content of feldspar and biotite and the macroscale Young's modulus. Meanwhile, the macroscale Young's modulus of granites has a negative correlation with the content of quartz and weathering products. Unlike pre-existing references, we emphasize that the negative correlation between quartz content and macroscale Young's modulus is conditional and applicable only to granites with varying degrees of weathering. A theoretical model for the weathering-induced quartz content variation is shown in Fig. 17. During the weathering process,



(a) Sample-I (Tang et al. 2022)

(b) Sample-II

(c) Sample-III

Fig. 13 Young's modulus results of biotite using nanoindentation testing

feldspar and biotite transform into weathering products. These weathering products are frequently carried away by some physical weathering processes, such fluid flow, which generates microdefects. Then, these microdefects disappear under compression loading, such as geostress, which leads to the reduction of total volume and the increase of quartz content.

6 Conclusions

The four granitic samples with different weathering degrees were collected. The Sample I is fresh granitic rock, Sample II is slightly weathered, the Sample III is moderately weathered, and Sample IV is completely weathered. The following conclusions can be achieved:

(1) Quartz is erosionally resistant compared to feldspar and biotite. The weathering product of feldspar is sericite, and the weathering product of biotite is chlorite. During the weathering process, the volume fractions of quartz and weathering products increase, however the volume fractions of feldspar and biotite decrease.

(2) During the weathering process, microdefects increase significantly, including pores and microcracks. Weathering effect leads to the fragmentation of minerals, and microcracks mainly distribute in the area when weathering products accumulate.

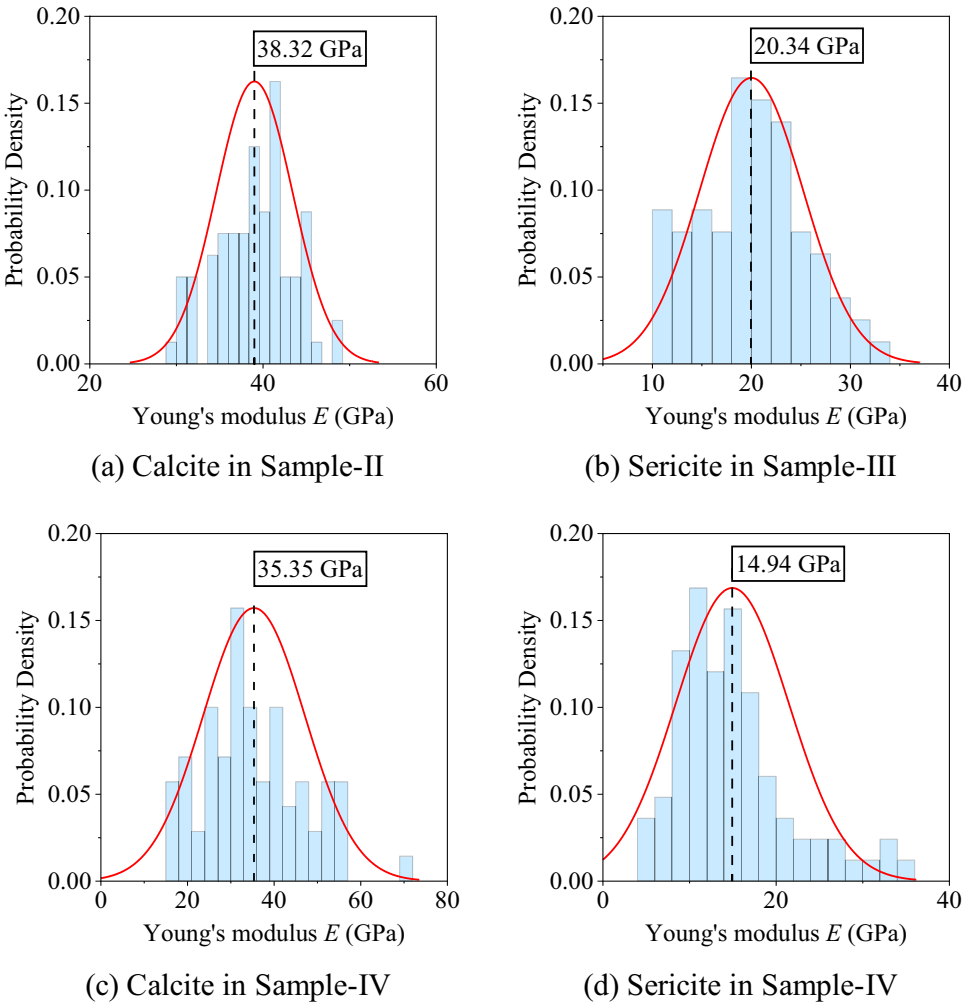


Fig. 14 Young's modulus results of weathering products using nanoindentation testing

Table 3 Macroscale mechanical properties of four samples

	Sample-I	Sample-II	Sample-III	Sample-IV
Density (kg/m^3)	2642.2	2587.54	2537.18	/
Poisson's ratio	/	0.139	0.446	/
Young's modulus (GPa)	41.78	20.45	14.58	10.52

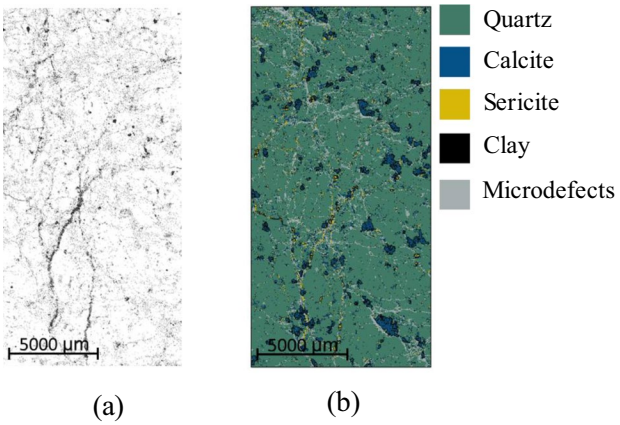


Fig. 15 Generating AGBM of Sample-IV based on the result of micro-RME **a** TIMA image; **b** Accurate grain-based model

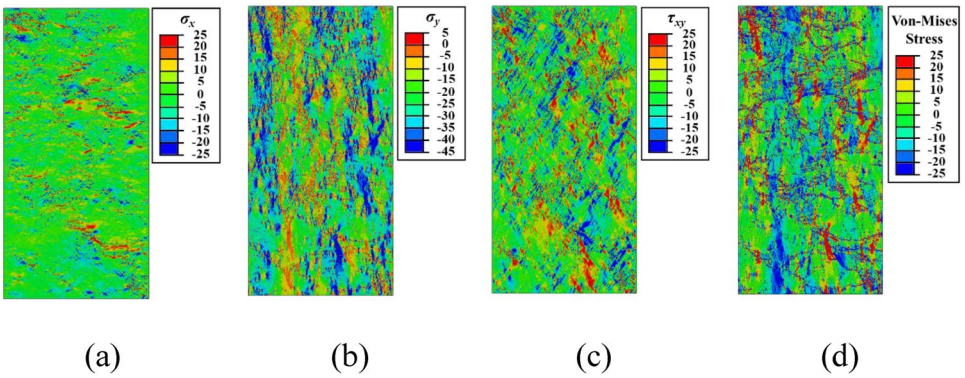


Fig. 16 Simulated stress distribution in Sample IV. The σ_x and σ_y are stress in x- and y-direction, respectively. τ_{xy} is the shear stress

Table 4 The Pearson correlation coefficient of different indexes

	Quartz	Feldspar	Biotite	Weathering products	Microdefects	Young's modulus
Quartz	1	−0.965	−0.903	0.434	0.536	−0.981
Feldspar	−0.965	1	0.981	−0.654	−0.737	0.992
Biotite	−0.903	0.981	1	−0.777	−0.832	0.950
Weathering products	0.434	−0.654	−0.777	1	0.982	−0.572
Microdefects	0.536	−0.737	−0.832	0.982	1	−0.676
Young's modulus	−0.981	0.992	0.950	−0.572	−0.676	1

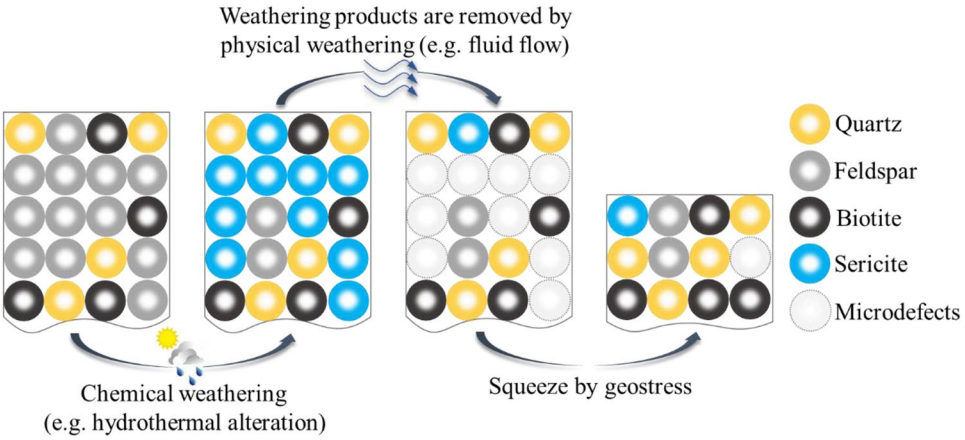


Fig. 17 Weathering process coupled by chemical and physical weathering in granite

(3) During the weathering process, Young's modulus of quartz and feldspar almost keeps constant, however, Young's modulus of biotite decreases significantly.
(4) From the viewpoint of the weathering effect, we observed a negative correlation between quartz content and macroscale Young's modulus.

Acknowledgements This work was supported by the National Natural Science Foundation of China No.12172264 and Basic Research Program of Central Government Funds for Shenzhen Science and Technology Development (2021Szvup103).

Author contribution JQ: Experiments, Writing-original draft. MN: Investigation, Writing-review & editing. QZ: Writing-review & editing. QL: Writing-review & editing. XT: Supervision, Methodology, Writing-review & editing.

Funding This research was supported by National Natural Science Foundation of China (Grant 12172264).

Data availability The data are available from the corresponding author on reasonable request.

Declarations

Conflict of Interest The authors declare that they have no known competing financial interests or personal relationships that could have appeared to influence the work reported in this paper.

References

Abad SANK, Tugrul A, Gokceoglu C, Armaghani DJ (2016) Characteristics of weathering zones of granitic rocks in Malaysia for geotechnical engineering design. Eng Geol 200:94–103. https://doi.org/10.1016/j.enggeo.2015.12.006

Askaripour M, Saeidi A, Mercier-Langevin P, Rouleau A (2022) A review of relationship between texture characteristic and mechanical properties of rock. Geotechnics 2(1):262–296. https://doi.org/10.3390/geotechnics2010012

Basu A, Celestino TB, Bortolucci AA (2009) Evaluation of rock mechanical behaviors under uniaxial compression with reference to assessed weathering grades. Rock Mech Rock Eng 42:73–93. https://doi.org/10.1007/s00603-008-0170-2

Chen X, Yu J, Tang CA, Li H, Wang SY (2017) Experimental and numerical investigation of permeability evolution with damage of sandstone under triaxial compression. Rock Mech Rock Eng 50:1529–1549. https://doi.org/10.1007/s00603-017-1169-3

Du K, Sun Y, Zhou J, Khandelwal M, Gong FQ (2022) Mineral composition and grain size effects on the fracture and acoustic emission (AE) characteristics of rocks under compressive and tensile stress. Rock Mech Rock Eng 55:6445–6474. https://doi.org/10.1007/s00603-022-02980-y

Fairhurst CE, Hudson JA (1999) Draft ISRM suggested method for the complete stressstrain curve for the intact rock in uniaxial compression. Int J Rock Mech Min Sci 36(3):279–289

Hassan NF, Jimoh OA, Shehu SA, Hareyani Z (2019) The effect of mineralogical composition on strength and drillability of granitic rocks in Hulu Langat, Selangor Malaysia. Geotech Geol Eng 37:5499–5505. https://doi.org/10.1007/s10706-019-00995-x

Heidari M, Momeni AA, Naseri F (2013) New weathering classifications for granitic rocks based on physico-mechanical parameters. Eng Geol 166:65–73. https://doi.org/10.1016/j.enggeo.2013.08.007

Hrstka T, Gottlieb P, Skala R, Breiter K, Motl D (2018) Automated mineralogy and petrology-applications of TESCAN Integrated Mineral Analyzer (TIMA). J Geosci 63(1):47–63. https://doi.org/10.3190/jgeosci.250

Huang XL, Qi SW, Zheng BW, Liang N, Li LH, Xue L, Guo SF, Sun X, Tai DP (2021) An advanced grain-based model to characterize mechanical behaviors of crystalline rocks with different weathering degrees. Eng Geol 280:105951. https://doi.org/10.1016/j.enggeo.2020.105951

Jacob SR, Wellington DF, Bell JFIII, Achilles C, Fraeman AA, Horgan B et al (2020) Spectral, compositional, and physical properties of the upper murray formation and vera rubin ridge, gale crater, mars. J Geophys Res Planets 125:e2019JE006290. https://doi.org/10.1029/2019JE006290

Kanno H, Moriguchi SJ, Tsuda Y, Yoshida I, Iwanaga SJ, Terada K (2023) A method for rockfall risk quantification and optimal arrangement of protection structures along a road. Eng Geol 314:5. https://doi.org/10.1016/j.enggeo.2023.107004

Lan HX, Martin CD, Hu B (2010) Effect of heterogeneity of brittle rock on micromechanical extensile behavior during compression loading. J Geophys Res Solid Earth 115:B1. https://doi.org/10.1029/2009JB006496

Li Y, Luo S, Lu M, Wu YK, Zhou N, Wang DF, Lu YH, Zhang GP (2021) Cross-scale characterization of sandstones via statistical nanoindentation: evaluation of data analytics and upscaling models. Int J Rock Mech Min 142:104738. https://doi.org/10.1016/j.ijrmms.2021.104738

Liu XY, Zhang XW, Kong LW, Wang G, Lu JF (2022) Disintegration of granite residual soils with varying degrees of weathering. Eng Geol 305:106723. https://doi.org/10.1016/j.enggeo.2022.106723

Luo S, Lu Y, Wu Y, Song J, DeGroot DJ, Jin Y, Zhang GP (2020) Cross-scale characterization of the elasticity of shales:statistical nanoindentation and data analytics. J Mech Phys Solid 140:103945. https://doi.org/10.1016/j.jmps.2020.103945

Mahabadi OK, Randall NX, Zong Z, Grasselli G (2012) A novel approach for micro-scale characterization and modeling of geomaterials incorporating actual material heterogeneity. Geophys Res Lett 39:L01303. https://doi.org/10.1029/2011GL050411

Mahabadi OK, Tatone BSA, Grasselli G (2014) Influence of microscale heterogeneity and microstructure on the tensile behavior of crystalline rocks. J Geophys Res 119(7):5324–5341. https://doi.org/10.1002/2014JB011064

Martin RP, Henchert SR (1986) Principles for description and classification ofweathered rock for engineering purposes. Geol Soc Eng Geol Spec Publ 2:299–308. https://doi.org/10.1144/GSL.1986.002.01.53

Moye DG (1955) Engineering geology for the snowy mountain scheme. J Inst Eng (aust) 27:281–299

Oliver WC, Pharr GM (1992) An improved technique for determining hardness and elastic modulus using load and displacement sensing indentation experiments. J Mater Res 7:1564–1583. https://doi.org/10.1557/JMR.1992.1564

Oyen ML (2013) Nanoindentation of biological and biomimetic materials. Exp Tech 37(1):73–87. https://doi.org/10.1111/j.1747-1567.2011.00716.x

Peng J, Wong LNY, Teh CI (2017) Influence of grain size heterogeneity on strength and microcracking behavior of crystalline rocks. J Geophys Res Solid Earth 122(2):1054–1073. https://doi.org/10.1002/2016JB013469

Peng J, Wong LNY, Teh CI, Li Z (2018) Modeling micro-cracking behavior of Bukit Timah granite using grain-based model. Rock Mech Rock Eng 51:135–154. https://doi.org/10.1007/s00603-017-1316-x

Peters GH, Carey EM, Anderson RC, Abbey WJ, Kinnett R, Watkins JA et al (2018) Uniaxial compressive strengths of rocks drilled at Gale crater, Mars. Geophys Res Lett 45:108–116. https://doi.org/10.1002/2017GL075965

Randall N, Vandamme M, Ulm F (2009) Nanoindentation analysis as a two-dimensional tool for mapping the mechanical properties of complex surfaces. J Mater Res 24(3):679–690. https://doi.org/10.1557/jmr.2009.0149

Sajid M, Arif M, Shah MT (2014) Petrogenesis of granites from the Utla area of Gadoon, north-west Pakistan: Implications from petrography and geochemistry. J Earth Sci 25:445–459. https://doi.org/10.1007/s12583-014-0435-5

Santoro L, Boni M, Rollinson GK, Mondillo N, Balassone G, Clegg AM (2014) Mineralogical characterization of the Hakkari nonsulfide Zn(Pb) deposit (Turkey): the benefits of QEMSCAN®. Minerals Eng 69:29–39. https://doi.org/10.1016/j.mineng.2014.07.002

Sousa LMO (2013) The influence of the characteristics of quartz and mineral deterioration on the strength of granitic dimensional stones. Environ Earth Sci 69:1333–1346. https://doi.org/10.1007/s12665-012-2036-x

Tang XH, Tao SJ, Li P, Rutqvist J, Hu MS, Sun L (2022a) The propagation and interaction of cracks under freeze-thaw cycling in rock-like material. Int J Rock Mech Min Sci 154:105112. https://doi.org/10.1016/j.ijrmms.2022.105112

Tang XH, Zhang YH, Xu JJ, Rutqvist J, Hu MS, Wang ZZ, Liu QS (2022b) Determining Young's modulus of granite using accurate grain-based modeling with microscale rock mechanical experiments. Int J Rock Mech Min Sci 157:105167. https://doi.org/10.1016/j.ijrmms.2022.105167

Tang XH, Xu JJ, Zhang YH, Zhao H, Paluszny A, Wan X, Wang ZZ (2023) The rock-forming minerals and macroscale mechanical properties of asteroid rocks. Eng Geol 321:107154. https://doi.org/10.1016/j.enggeo.2023.107154

Wang P, Xu JY, Liu SH, Wang HY (2016) Dynamic mechanical properties and deterioration of red-sandstone subjected to repeated thermal shocks. Eng Geol 212:44–52. https://doi.org/10.1016/j.enggeo.2016.07.015

Witze A (2021a) Why NASA's Mars rover failed to collect its first rock core. Nature. https://doi.org/10.1038/d41586-021-02208-z

Witze A (2021b) Success! Mars rover finally collects its first rock core. Nature 597(7876):317–317. https://doi.org/10.1038/d41586-021-02394-w

Wong LNY, Maruvanchery V (2016) Different lithological varieties of Bukit Timah granite in Singapore: a preliminary comparison study on engineering properties. Rock Mech Rock Eng 49:2923–2935. https://doi.org/10.1007/s00603-015-0825-8

Xu JJ, Tang XH, Wang ZZ, Feng YF, Bian K (2020) Investigating the softening of weak interlayers during landslides using nanoindentation experiments and simulations. Eng Geol 277:10580. https://doi.org/10.1016/j.enggeo.2020.105801

Xu JJ, Zhang YH, Rutqvist J, Hu MS, Wang ZZ, Tang XH (2023) Thermally induced microcracks in granite and their effect on the macroscale mechanical behavior. J Geophys Res Solid Earth 128:e2022JB024920. https://doi.org/10.1029/2022JB024920

Yang SQ, Yin PF, Huang YH (2019) Experiment and discrete element modelling on strength, deformation and failure behaviour of shale under brazilian compression. Rock Mech Rock Eng 52:4339–4359. https://doi.org/10.1007/s00603-019-01847-z

Zhang JH, Hu LM, Pant R, Yu YZ, Wei ZX, Zhang GP (2013) Effects of interlayer interactions on the nanoindentation behavior and hardness of 2:1 phyllosilicates. Appl Clay Sci 80–81:267–280. https://doi.org/10.1016/j.clay.2013.04.013

Zhou ZL, Ullah B, Rui YC, Cai X, Lu JY (2023) Predicting the failure of different rocks subjected to freeze-thaw weathering using critical slowing down theory on acoustic emission characteristics. Eng Geol 316:107059. https://doi.org/10.1016/j.enggeo.2023.107059

Publisher's Note Springer Nature remains neutral with regard to jurisdictional claims in published maps and institutional affiliations.

Springer Nature or its licensor (e.g. a society or other partner) holds exclusive rights to this article under a publishing agreement with the author(s) or other rightsholder(s); author self-archiving of the accepted manuscript version of this article is solely governed by the terms of such publishing agreement and applicable law.